AIP | Review of Scientific Instruments

Generation of circularly polarized radiation from a compact plasma-based extreme ultraviolet light source for tabletop X-ray magnetic circular dichroism studies

Daniel Wilson, Denis Rudolf, Christian Weier, Roman Adam, Gerrit Winkler, Robert Frömter, Serhiy Danylyuk, Klaus Bergmann, Detlev Grützmacher, Claus M. Schneider, and Larissa Juschkin

Citation: Review of Scientific Instruments **85**, 103110 (2014); doi: 10.1063/1.4897491
View online: http://dx.doi.org/10.1063/1.4897491
View Table of Contents: http://scitation.aip.org/content/aip/journal/rsi/85/10?ver=pdfcov
Published by the AIP Publishing

Generation of circularly polarized radiation from a compact plasma-based extreme ultraviolet light source for tabletop X-ray magnetic circular dichroism studies

Daniel Wilson,[1,2,a)] Denis Rudolf,[1,2,a),b)] Christian Weier,[3] Roman Adam,[3] Gerrit Winkler,[4] Robert Frömter,[4] Serhiy Danylyuk,[5] Klaus Bergmann,[6] Detlev Grützmacher,[2] Claus M. Schneider,[3] and Larissa Juschkin[1,2]

[1]*RWTH Aachen University, Experimental Physics of EUV, Steinbachstraße 15, 52074 Aachen, Germany*
[2]*Forschungszentrum Jülich GmbH, Peter Grünberg Institut (PGI-9), JARA-FIT, 52425 Jülich, Germany*
[3]*Forschungszentrum Jülich GmbH, Peter Grünberg Institut (PGI-6), JARA-FIT, 52425 Jülich, Germany*
[4]*Institut für Angewandte Physik, Universität Hamburg, Jungiusstraße 11, 20355 Hamburg, Germany*
[5]*RWTH Aachen University, Chair for Technology of Optical Systems, JARA-FIT, Steinbachstraße 15, 52074 Aachen, Germany*
[6]*Fraunhofer Institute for Laser Technology, Steinbachstrasse 15, 52074 Aachen, Germany*

(Received 1 September 2014; accepted 27 September 2014; published online 16 October 2014)

Generation of circularly polarized light in the extreme ultraviolet (EUV) spectral region (about 25 eV–250 eV) is highly desirable for applications in spectroscopy and microscopy but very challenging to achieve in a small-scale laboratory. We present a compact apparatus for generation of linearly and circularly polarized EUV radiation from a gas-discharge plasma light source between 50 eV and 70 eV photon energy. In this spectral range, the 3*p* absorption edges of Fe (54 eV), Co (60 eV), and Ni (67 eV) offer a high magnetic contrast often employed for magneto-optical and electron spectroscopy as well as for magnetic imaging. We simulated and designed an instrument for generation of linearly and circularly polarized EUV radiation and performed polarimetric measurements of the degree of linear and circular polarization. Furthermore, we demonstrate first measurements of the X-ray magnetic circular dichroism at the Co 3*p* absorption edge with a plasma-based EUV light source. Our approach opens the door for laboratory-based, element-selective spectroscopy of magnetic materials and spectro-microscopy of ferromagnetic domains. © *2014 AIP Publishing LLC*. [http://dx.doi.org/10.1063/1.4897491]

I. INTRODUCTION

Extreme ultraviolet (EUV) and soft X-ray spectral region extends from about 25 eV to 12 000 eV and is dominated by strong light-matter interaction.[1] The presence of absorption edges of every element allows strong elemental and chemical selectivity. In particular, linearly and circularly polarized EUV and soft X-ray radiation is highly desired for applications, such as reflectometry, ellipsometry, lithography, magneto-optical spectroscopy, and photoemission studies. In reflectometry, linearly polarized light is used for the characterization of EUV optics, such as multilayer Bragg mirrors.[2] In interference lithography, the contrast between the highest and lowest intensity in the resist is considerably better with linearly polarized light compared to unpolarized light.[3] Another application of polarized EUV and soft X-ray radiation, magneto-optical polarization spectroscopy,[4–6] provides valuable information about magneto-optical constants and enables studies of element- and layer-selective magnetization. For magneto-optical spectroscopy, both linearly and circularly polarized light is required.

In particular, X-ray magnetic circular dichroism (XMCD) is frequently used for magneto-optical and photoemission spectroscopy at the 2*p* (700 eV–860 eV) and 3*p* (50 eV–70 eV) absorption edges of Fe, Co, and Ni.[4–8]

Linearly and circularly polarized EUV and soft X-ray radiation is routinely generated at large-scale facilities such as electron storage rings and free-electron lasers – unique sources of high energy photons in terms of intensity, photon energy range, spectral bandwidth, pulse duration, and polarization. Therefore, a complete polarization analysis is usually performed at synchrotrons with sophisticated polarimetric and ellipsometric instruments.[9–11]

In a small-scale laboratory, various EUV and soft X-ray light sources are available, but only few of them are *a priori* polarized. While linearly polarized EUV light is routinely generated by intense ultrashort laser pulses,[12] only few attempts to either polarize EUV radiation circularly[13,14] or directly generate circular EUV radiation from a femtosecond laser[15] have been reported from laboratory-based experiments. A straightforward concept for conversion of linear to circular EUV polarization is to exploit the phase shift between the s- and p-components of light upon reflection from a flat surface. For that purpose, a phase shift of $\pm 90^\circ$ between the s- and p-components and identical reflectivity for the s- and p-components are required.[13,14,16,17] Laboratory-based instruments for generation of circularly polarized EUV light employ up to four mirrors. Due to the low overall reflectivity of a few percent in the EUV spectral range a sufficiently intense

[a)]D. Wilson and D. Rudolf contributed equally to this work.
[b)]Author to whom correspondence should be addressed. Electronic mail: d.rudolf@fz-juelich.de

EUV light source is required to obtain a reasonable photon flux after the conversion.

For our studies, we employ an intense gas-discharge plasma-based EUV light source.[18–20] The multiply ionized atoms, in our case oxygen and nitrogen ions, emit narrow-bandwidth spectral lines ($\Delta E/E = 10^{-3}-10^{-5}$, where E is the photon energy) in the photon energy range between vacuum ultraviolet and soft X-rays. We optimized the EUV light source for operation above 50 eV photon energy. To linearly polarize the initially unpolarized EUV light and simultaneously select emission lines around the 3*p* absorption edge of Co (60 eV), we designed a Bragg mirror linear polarizer operating close to the Brewster angle. Behind the linear polarizer, we placed a broadband triple-reflection circular polarizer, which covers the 3*p* absorption edges of Fe, Co, and Ni between 50 eV and 70 eV.

To our knowledge, for the first time in a laboratory-based experiment with a plasma-based EUV light source, we demonstrate XMCD measurements on Co/Pt-multilayer films at the Co 3*p* absorption edge.

Our paper is structured as follows. In Sec. II, we present the simulation and design of the instrument for generation of circularly polarized EUV radiation covering the 3*p* absorption edges of Fe, Co, and Ni. In Sec. III, we describe the spectral reflectivity of the Bragg mirror linear polarizer designed to reflect emission lines around the Co 3*p* absorption edge. In Sec. IV, we analyze the performance of linear and circular polarizer around 60.5 eV extracted from polarimetric measurements. Finally in Sec. V, we present X-ray magnetic circular dichroism measurements on Co/Pt-multilayers at the Co 3*p* absorption edge.

II. SIMULATION AND DESIGN OF THE INSTRUMENT FOR GENERATION OF CIRCULARLY POLARIZED EUV RADIATION AT THE 3*p* ABSORPTION EDGES OF IRON, COBALT, AND NICKEL

A. Simulation based on Stokes formalism

The concept of experimental apparatus to generate circularly polarized light at the 3*p* absorption edges of Fe, Co and Ni and to measure the degree of circular polarization is presented in Fig. 1. We refer to the angle notation of Fig. 1 for further discussion of the simulation and experimental results.

To simulate and design the instrument for generation of circularly polarized light between 50 eV and 70 eV, we applied the Stokes polarization formalism[13,14,21] for our specific case. The four Stokes parameters are

$$\begin{aligned} S_0 &= E_p^2 + E_s^2, \\ S_1 &= E_p^2 - E_s^2, \\ S_2 &= 2E_p E_s \cos(\Delta), \\ S_3 &= -2E_p E_s \sin(\Delta), \end{aligned} \tag{1}$$

which include the amplitudes of s- and p-polarized light E_s and E_p and the phase shift Δ between them describing the complete polarization state of light.[21] To measure the degree of linear (p_L) and circular (p_C) polarization, we define

$$p_L = \frac{S_1}{S_0} \tag{2}$$

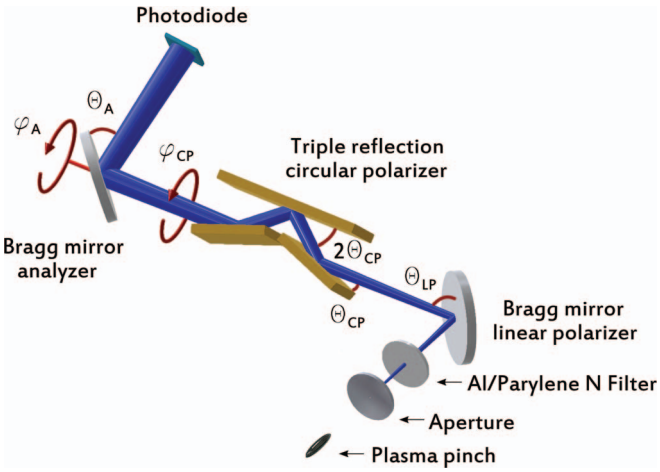

FIG. 1. The EUV light at the 3*p* absorption edge of Co (60 eV) emitted by the oxygen plasma first passes through an aperture and Al/Parylene N filter. Then the light is linearly (s) polarized by a Bragg mirror placed at the Brewster angle θ_{LP}. The linearly polarized light is reflected by three mirrors whose rotation angle φ_{CP} is adjusted to create circular polarization. The polarization state of light is observed by the Bragg mirror analyzer together with a photodiode, both rotatable around the beam axis (angle φ_A).

and

$$p_C = \frac{S_3}{S_0}. \tag{3}$$

Equation (2) assumes that the light is either completely s- or p-polarized ($S_2 = 0$). Moreover, Eqs. (2) and (3) distinguish between s ($p_L = -1$)- and p ($p_L = +1$)-polarization as well as between positive ($p_C = +1$) and negative ($p_C = -1$) helicity (right- and left-circularly polarized light), respectively.

Each optical element, represented by a 4 × 4 so-called Müller matrix, has a different reflection or transmission for the s- and p-component and, in addition to that, it causes a phase shift between the two components. To characterize the polarization state of light, in our case after reflection, the two parameters ψ_r (rotation of the main ellipse axis) and Δ_r (phase shift between the s- and p-component) are fundamental quantities for ellipsometric studies.[21] For complex-valued s- and p-reflectivities r_s and r_p, the ellipsometric relationship reads

$$\tan(\psi_r) \times e^{i\Delta_r} = \frac{r_p}{r_s}. \tag{4}$$

The s- and p-reflectivities, readily calculated using Fresnel equations, depend on the refractive index (and thus the photon energy) as well as the angle of incidence. For our simulations, we extracted the complex-valued refractive indices for the EUV spectral range from the database of the Center of X-Ray Optics (CXRO).[22] Since the emitted radiation of our plasma discharge source is initially unpolarized, the light has to be polarized linearly first and then polarized circularly. To this end, we designed multilayer Bragg mirrors for Brewster angle operation and peak reflectivity at 53.9 eV (Fe 3*p*), 60.5 eV (Co 3*p*), and 67.0 eV (Ni 3*p*). The requirements for the linear polarizer are high reflectivity on one hand and high degree of linear polarization on the other hand, both at the 3*p* absorption edges of Fe, Co, and Ni. In addition to that, a

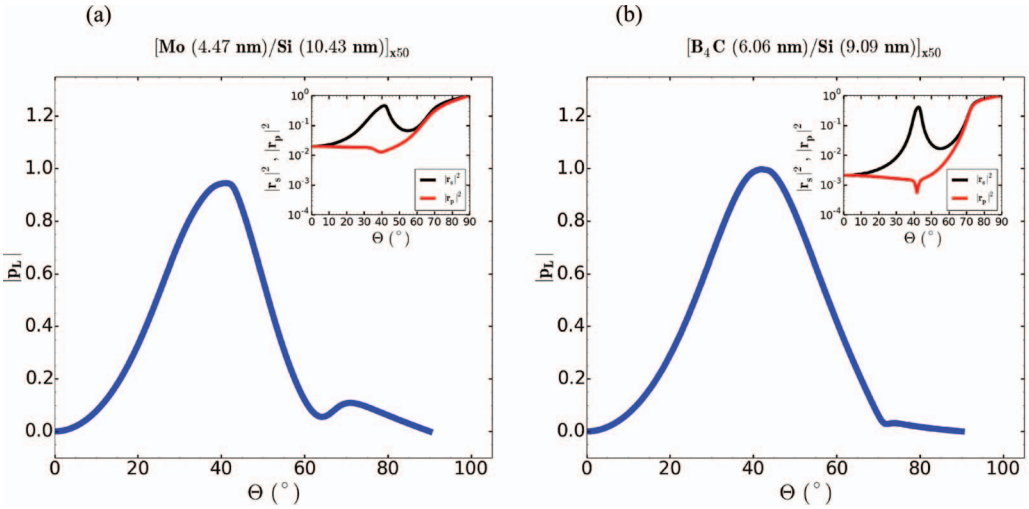

FIG. 2. The inset shows a comparison of reflectivity for s- and p-polarized light between the Mo/Si (a) and B_4C/Si (b) Bragg mirror linear polarizer at 60.5 eV photon energy ($3p$ absorption edge of Co). The simulated reflectivity for s- and p-polarized light (black and red lines) is plotted for different angles Θ with respect to normal incidence. The resulting degree of linear polarization p_L (blue line) is higher for B_4C/Si linear polarizer ($|p_L| = 1.00$) compared to Mo/Si linear polarizer ($|p_L| = 0.94$).

spectrally sufficiently narrow reflectivity peak is required to select single emission lines.

We simulated the Bragg mirror reflectivity based on the iterative algorithm from Ref. 21. In our simulations, we compared the s- and p-reflectivity of two material combinations, namely, Mo/Si and B_4C/Si at the $3p$ absorption edges of Fe, Co, and Ni (Fig. 2 for Co $3p$). For the B_4C/Si Bragg mirror linear polarizer, our simulation shows a higher ratio between the s- and p-reflectivity in the vicinity of the Brewster angle compared to the Mo/Si linear polarizer. Due to the high degree of linear polarization p_L close to 1 and also due to a sufficiently narrow bandwidth (1.36 nm for Co $3p$, see Table I), we used the B_4C/Si Bragg mirror linear polarizer in our experiments. We summarize the most important parameters of the B_4C/Si Bragg mirrors in Table I. In Fig. 2, we display the simulation results for the $3p$ absorption edge of Co (60 eV). For the $3p$ absorption edges of Fe and Ni, the simulation results are similar in terms of magnitude and shape of the p_L-Θ graph.

In the next step, we simulated the degree of circular polarization due to the phase shift Δ between the s- and p-components of the electric field upon reflection. Reported concepts of a circular polarizer between 50 eV and 70 eV photon energy[14,16] are based on four non-rotatable mirrors to create a phase shift $\Delta = \pm 90°$.

TABLE I. Parameters of the B_4C/Si multilayer mirror linear polarizers for the $3p$ absorption edges of Fe (53.9 eV), Co (60.5 eV), and Ni (67.0 eV). E denotes the photon energy, θ_B the Brewster angle (with respect to normal incidence), R_s and R_p the s- and p-reflectivities, and p_L the degree of linear polarization after reflection.

	$[B_4C$ (5.36 nm)/ Si (8.04 nm)$]_{x50}$	$[B_4C$ (6.06 nm)/ Si (9.09 nm)$]_{x50}$	$[B_4C$ (6.72 nm)/ Si (10.08 nm)$]_{x50}$
E (eV)	67.0	60.5	53.9
θ_B (deg)	42.79	42.52	40.81
R_s	0.41	0.42	0.39
R_p	0.96×10^{-3}	0.26×10^{-3}	0.72×10^{-3}
$FWHM$ of R_s (nm)	1.05	1.36	1.71
p_L	−0.999	−0.995	−0.996

To fulfill the requirements of high degree of circular polarization p_C, high overall reflectivity of the circular polarizer between 50 eV and 70 eV, and a simple rotation around the beam axis without any beam movement, we used three instead of four mirrors.[23]

For 20 nm Mo on Si, we found the triple-reflection at 20°–40°–20° grazing incidence to give the highest $|p_C|$ of >0.99 at 60.5 eV. The total phase shift after three reflections amounts to $\Delta_{CP} = -90.9°$. The degree of circular polarization p_C depends on the rotation angle φ_{CP} (see Fig. 1) and amounts to $p_C = +1$ (right circular) for $\varphi_{CP} \approx 70°$ (250°) and to $p_C = -1$ (left circular) for $\varphi_{CP} \approx 110°$ (290°) for the $3p$ absorption edges of Fe, Co, and Ni (Fig. 3). Therefore, the circular polarizer offers two main advantages. First, the helicity of light is readily changed between left and right circular polarization. Second, only one circular polarizer covers all $3p$ absorption edges of the $3d$ ferromagnets and therefore enables magneto-optical polarization spectroscopy and microscopy of Fe, Co, and Ni taking advantage of the XMCD effect. The overall reflectivity R_{CP} of the circular polarizer at the $3p$ absorption edges of Fe, Co, and Ni starting from fully s-polarized light is displayed in Fig. 3(b). For $p_C = 1$ ($\varphi_{CP} = 70°$), it amounts to about 1%. Our result is comparable to the overall reflectivity obtained with the four mirror configuration.[14,16]

To measure the degree of linear and circular polarization, we used a Bragg mirror analyzer and a photodiode, which we rotated around the beam axis in the Rabinovitch polarimeter configuration.[24] The requirements for the Bragg mirror analyzer are the same as for the linear polarizer (high reflectivity, high degree of linear polarization, narrow bandwidth) and therefore, we used two identical Bragg mirrors for linear polarizer and analyzer.

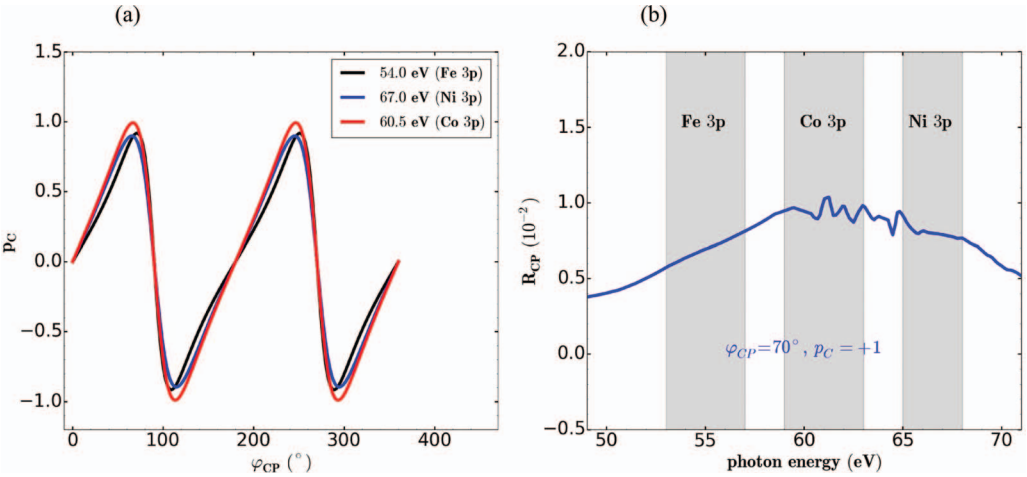

FIG. 3. (a) Simulated degree of circular polarization p_C after the circular polarizer as a function of rotation angle φ_{CP} for three photon energies corresponding to the 3*p* absorption edges of Fe, Co, and Ni. The circular polarizer was optimized for the Co 3*p* absorption edge, thus showing the highest degree of circular polarization for $\varphi_{CP} \approx 70°, 250°$ ($p_C = +1$), and $\varphi_{CP} \approx 110°, 290°$ ($p_C = -1$). (b) Overall reflectivity R_{CP} of the circular polarizer for $p_C = +1$ around the 3*p* absorption edges of Fe, Co, and Ni with a strong magneto-optical signal[6] (grey boxes).

B. Design of the instrument for generation and analysis of polarized EUV light and circular magnetic dichroism measurements between 50 eV and 70 eV photon energy

The entire optical setup is mounted on an optical breadboard inside a vacuum chamber. For the Bragg mirror linear polarizer, we used a commercial piezo-driven, vacuum-compatible holder for 1 in. mirrors (Smaract STT-25). During the alignment, the holder allows for tilting the mirror around the vertical and horizontal axes by ± 2.5°.

The subsequent optical element, the triple-reflection circular polarizer, required a specially designed holder for fixed mounting of three mirrors (two mirrors 10 mm × 30 mm, one mirror 10 mm × 23 mm) for 20°–40°–20° grazing incidence.[23] Thus, no further relative alignment of the mirrors is necessary. The holder consists of two parts secured together using screws (Fig. 4). Inside the cutouts of the two parts (two cutouts in one part, one cutout in the other part) the mirrors consisting of 20 nm Mo layer thermally evaporated on Si substrate are attached using glue. The entire device is mounted on a piezo-driven, vacuum-compatible rotational stage (Smaract SR-7012-S, minimum step size of 0.2×10^{-3}°) with positioning control. For polarization analysis using a Rabinovitch polarimeter,[24] we designed a special Bragg mirror holder for 1 in. optics allowing 42° incidence angle with respect to the normal (Fig. 4) corresponding to the Brewster angle at 60.5 eV (Co 3*p* absorption edge). Similar to the triple-reflection circular polarizer, the holder is mounted on a piezo-driven, vacuum-compatible rotational stage (Smaract SR-5714-S, minimum step size of 0.16×10^{-3}°) equipped with positioning sensors. We also designed a holder for the AXUV 100G photodiode (10 mm × 10 mm active area) with mechanical support for the electrical SMA connector. The photodiode holder is attached to the analyzer holder and rotates with the analyzer around the beam axis.

All optical elements were prealigned using visible light. We performed the angular alignment of the Bragg mirror linear polarizer optimizing the reflectivity at 60.5 eV. For that purpose, we rotated the vacuum chamber around the central axis in the surface plane of the linear polarizer simultaneously recording EUV spectra. Once the intensity of emission lines

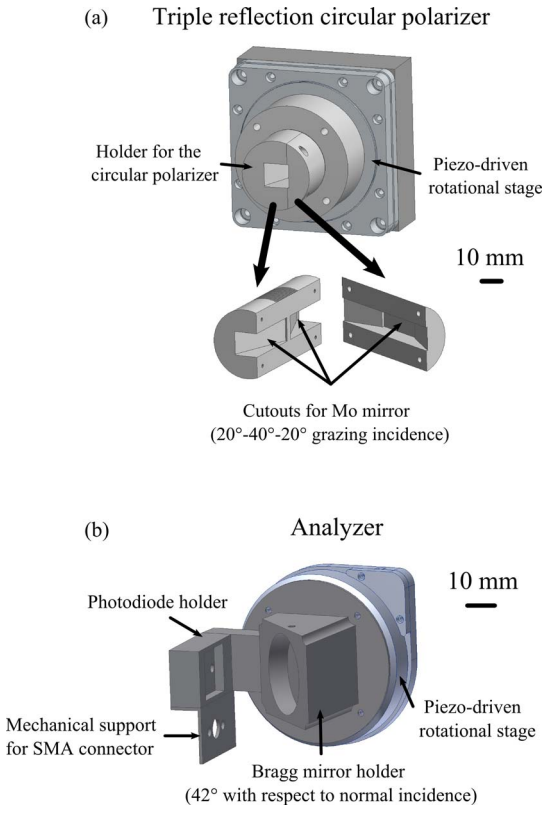

FIG. 4. (a) Holder for the triple reflection circular polarizer consisting of two halves. All mirrors comprising a Mo (20 nm) layer on Si substrate are glued inside the milled parts. The whole device is attached to a piezo-driven rotational stage with positioning sensors. (b) Analyzer consisting of a Bragg mirror holder for 42° with respect to the normal incidence (Brewster angle at 60.5 eV) and a photodiode holder. The whole device mounted on a piezo-driven rotational stage with positioning control is rotated around the beam axis (Rabinovitch polarimeter[24]).

at 60.5 eV was highest, the alignment goal was reached. We note that the linear polarizer accepts a wide angle range between $\Theta = 35^\circ$ and $\Theta = 50^\circ$ without significant loss of the degree of linear polarization (Fig. 2(b), blue curve).

For X-ray magnetic circular dichroism measurements at the Co 3*p* absorption edge, we removed the Bragg mirror analyzer and placed a Co/Pt multilayer sample between the pole shoes of a ferromagnetic yoke to magnetize it. We designed the yoke with a bore hole of 2 mm diameter for transmission measurements and magnetized the soft ferromagnetic yoke by a coil wound around the yoke. When supplying 4 A current to the coil, the magnetic field reaches a maximum of 320 mT between the pole shoes with a 2 mm gap.

For the Co/Pt multilayer sample (10 mm × 10 mm) with a Si_3N_4 window (0.5 mm × 0.5 mm), we designed a separate holder for transmission experiments. To align the Co/Pt multilayer sample between the pole shoes of the yoke, we placed the sample on a two-dimensional piezo-driven linear stage for vertical and horizontal movement.

III. CHARACTERIZATION OF THE PLASMA EMISSION SPECTRUM BEHIND THE BRAGG MIRROR LINEAR POLARIZER

For our measurements, we employed a gas-discharge plasma EUV light source developed at the Fraunhofer Institute for Laser Technology[18–20] and specifically designed for water window operation (280 eV–530 eV). In our experiments, the source parameters were 3.5 kV discharge voltage, 2 μF total capacity and 20 Hz pulse repetition rate. In order to produce high intensity radiation between 50 eV and 70 eV photon energy, we used EUV radiation emitted from highly ionized nitrogen (N^{3+}, N^{4+}) and oxygen atoms (O^{4+}, O^{5+}). A typical spectrum measured by a grazing-incidence EUV spectrometer with a blazed, spherical, gold-coated grating (1200 lines/mm) and a back-illuminated CCD camera (Andor iKon-M) is presented in Fig. 5. The measured relative spectral bandwidth of single emission lines $\Delta\lambda/\lambda \approx 10^{-3}$ is limited by the spectral resolution of our spectrometer. We note that emission lines of multiply ionized nitrogen and oxygen atoms are well in the range of 3*p* absorption edges of Fe, Co, and Ni. Furthermore, based on reported synchrotron measurements, the magneto-optical resonances are known to occur in the vicinity of the absorption edges and to be spectrally broader than the absorption edge itself, having a spectral width of few eV for the 3*p* absorption edges of Fe, Co, and Ni[5,6] (grey marked regions in Fig. 5 extracted from Ref. 6). Therefore, it is possible to use nitrogen and oxygen plasma radiation for element-selective magneto-optical polarization spectroscopy and microscopy at the 3*p* absorption edges of the 3*d* ferromagnets. In the case of Co, multiple emission lines of oxygen plasma are within the 3*p* magneto-optical resonance used in our magnetic circular dichroism measurements.

We selected oxygen and nitrogen emission lines by a Bragg mirror linear polarizer with peak reflectivity at 60.5 eV (Fig. 5(b)). The pulse energy of the oxygen and nitrogen emission lines around 60.5 eV measured with a calibrated EUV photodiode after the Bragg mirror is about 1.3 mJ/sr (1.4×10^{14} photons/sr) for the oxygen and 0.8 mJ/sr (0.8×10^{14} photons/sr) for the nitrogen plasma. To obtain the highest possible magnetic contrast in our XMCD studies, we used the oxygen instead of the nitrogen lines located very close to 60.5 eV (grey box in Fig. 5(b)). The intense oxygen line at 64.3 eV only contributes to the overall intensity but not to the magnetic signal.

IV. POLARIMETRIC MEASUREMENT OF THE DEGREE OF LINEAR AND CIRCULAR POLARIZATION AT 60 eV

We measured the polarization properties of EUV light around the 3*p* absorption edge of Co (60 eV) behind the linear and circular polarizer. Below we first describe the measurements of the degree of linear polarization and then that of circular polarization.

Similar to Eq. (2) in Sec. II A, we define the degree of linear polarization p_L after the linear polarizer as

$$p_L = \frac{S_{1,L}}{S_{0,L}}, \tag{5}$$

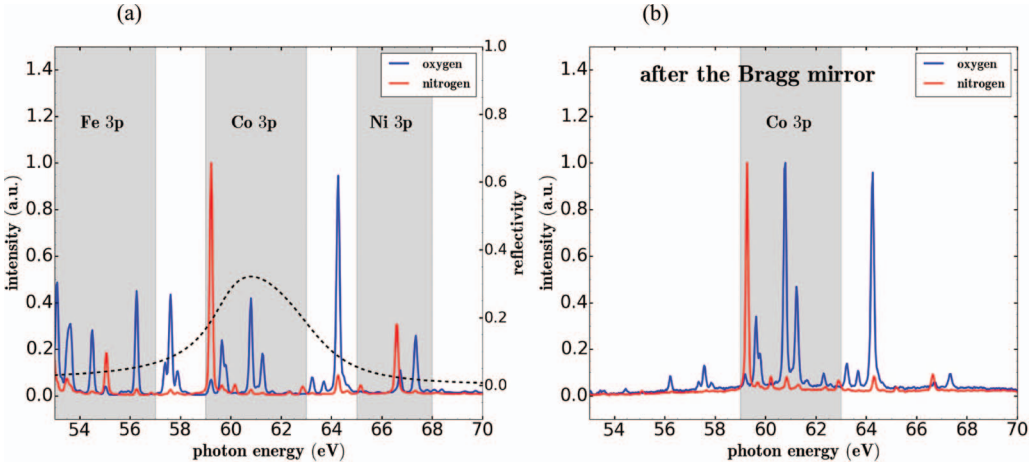

FIG. 5. (a) Spectra of highly ionized nitrogen (N^{3+}, N^{4+}) and oxygen (O^{4+}, O^{5+}) atoms between 53 eV and 70 eV as emitted from the gas-discharge plasma-based EUV light source. The grey boxes indicate the spectral region of magneto-optical resonances around the 3*p* absorption edges of Fe, Co, and Ni.[6] The dashed line corresponds to the reflectivity of the Bragg mirror linear polarizer for 60.5 eV at 42° normal incidence (Brewster angle). (b) Spectra of highly ionized nitrogen and oxygen atoms measured directly after the Bragg mirror linear polarizer for 60.5 eV comprising $[Si(9.09\ nm)/B_4C(6.06\ nm)]_{50x}$.

where $S_{0,L}$ and $S_{1,L}$ denote the first two values of the Stokes vector after the linear polarizer ($S_{2,L} = 0$). For completely s-polarized light, $p_L = -1$. The photodiode signal I_{LP} can be readily derived using the Stokes formalism and it reads

$$I_{LP}(\varphi_A) = I_{LP,0}[1 - p_L \times \cos(2\psi_A) \times \cos(\varphi_A)], \quad (6)$$

where $I_{LP,0}$ is a constant factor.

The influence of the analyzer is taken into account by

$$\psi_A = \tan^{-1}\left(\frac{|r_{p,A}|}{|r_{s,A}|}\right), \quad (7)$$

with $r_{p,A}$ and $r_{s,A}$ being the complex reflectivities for p- and s-polarized light. For our analyzer placed at the Brewster angle, we assume $|r_{p,A}|/|r_{s,A}| \approx 0$. Therefore, according to Eq. (7), $\psi_A \approx 0$ and thus $\cos(2\psi_A) = 1$. We define the analyzer rotation angle φ_A (Fig. 1) in such a way that for $\varphi_A = 0$ the s-p-coordinate systems of the linear polarizer and analyzer are identical and therefore $I_{LP}(\varphi_A = 0)$ is at maximum.

To measure the degree of linear polarization p_L (Eq. (5)), we placed the Bragg mirror analyzer directly behind the Bragg mirror linear polarizer and then rotated the analyzer clockwise with respect to the beam propagation direction around the beam axis by an angle φ_A (Fig. 6(a)). In order to suppress photon energies below 30 eV being also reflected by the Bragg mirror, we inserted an Al (100 nm)/Parylene N (100 nm) spectral filter into the beam path. We detected the signal by an EUV photodiode (AXUV 100G) and amplified with a low-noise current amplifier (FEMTO DLPCA-200) by a factor of 10^9 V/A. Finally, we measured the time-integrated voltage by a voltmeter (HP 3457A). For each angle position φ_A, we took an average of four measurements. In addition, we separately recorded the offset voltage for every angle position in order to correct our data for rotational stage position-dependent voltage variations. A representative measurement is shown in Fig. 6(a). We fitted multiple data sets according to Eq. (6) and obtained an average value of $p_L = -(0.94 \pm 0.04)$. Although the measured degree of linear polarization is slightly lower than predicted by simulations, it is sufficient for conversion of linearly to circularly polarized light.

To analyze the polarization properties of our triple-reflection circular polarizer, we modeled the Müller matrix of the circular polarizer as

$$M_{CP} = \begin{pmatrix} a & b & 0 & 0 \\ b & a & 0 & 0 \\ 0 & 0 & c \times \cos(\Delta_{CP}) & c \times \sin(\Delta_{CP}) \\ 0 & 0 & -c \times \sin(\Delta_{CP}) & c \times \cos(\Delta_{CP}) \end{pmatrix}. \quad (8)$$

The ansatz for the matrix M_{CP} stems from the multiplication of three standard Müller matrixes for all three Mo mirrors.[21] Here, the parameters a, b, and c depend on ellipsometric parameters ψ of the three Mo mirrors, whereas the parameter c depends on a and b, and can be readily determined from these parameters (see the Appendix). The phase shift Δ_{CP} denotes the total phase shift between the s- and p-component after all three reflections. The circular polarizer was designed for $\Delta_{CP} = -90.9°$ at 60.5 eV for efficient conversion of linearly to circularly polarized light (Sec. II A). The photodiode signal $I_{CP}(\varphi_A)$ behind the analyzer follows the equation

$$I_{CP}(\varphi_A) = I_{CP,0} \times [a - b \times \cos(2\varphi_{CP}) - b \times \cos(2\varphi_A + 2\varphi_{CP}) + 0.5 \times a \times \cos(2\varphi_A + 4\varphi_{CP}) + 0.5 \times a \times \cos(2\varphi_A)]. \quad (9)$$

Similar to Eq. (6), $I_{CP,0}$ is a constant factor, φ_A the rotation angle of the analyzer (clockwise with respect to the beam direction), and φ_{CP} the rotation angle of the circular polarizer (counterclockwise with respect to the beam direction). Equation (9) assumes a completely s-polarized light behind the linear polarizer, i.e., $S_{1,L} = -S_{0,L}$ and as before in Eq. (6), $\psi_A \approx 0$. Furthermore, we fixed $\Delta_{CP} = -90.9°$ and neglected small terms proportional to $c \cdot \cos(\Delta_{CP})$ in Eq. (9).

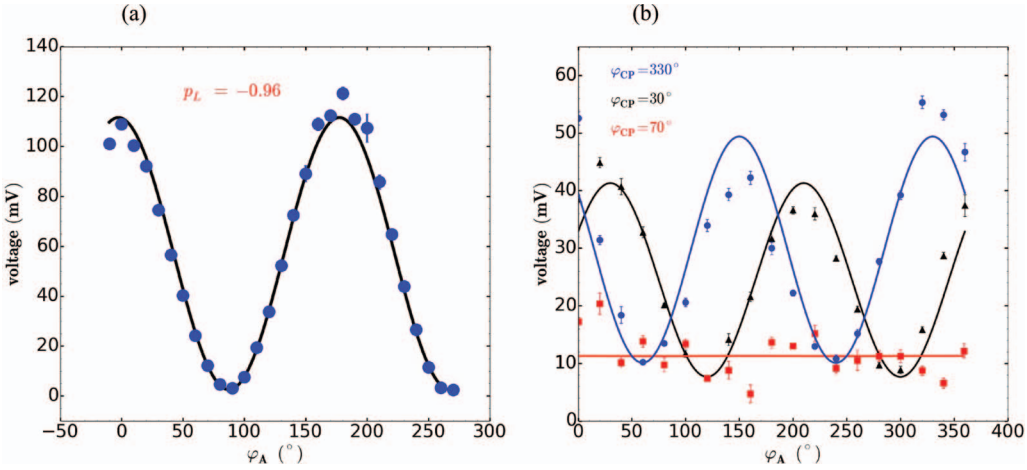

FIG. 6. (a) Measurement of the degree of linear polarization with emission lines from oxygen (Fig. 5(b)) around 60.5 eV photon energy (blue dots) and fit (black line) according to Eq. (6). The signal of the photodiode is plotted versus the analyzer rotation angle φ_A. The degree of linear polarization extracted from the fit amounts to $p_L = -0.96$. (b) Measurement of the degree of circular polarization with emission lines from oxygen around 60.5 eV behind the triple reflection circular polarizer. The photodiode voltage is shown as a function of the analyzer rotating angle φ_A (dots) for different rotation angles φ_{CP} of the circular polarizer. The lines are fits according to Eq. (9). For $\varphi_{CP} = 70°$ (red dots), the signal is independent of φ_A confirming that the degree of circular polarization is at maximum.

Fitting the measured intensity $I_{CP}(\varphi_A)$ from Eq. (9) for various fixed rotation angles φ_{CP} (Fig. 6(b)), we extracted the parameters a and b and then calculated the dependent parameter c. The details of our analysis are summarized in the Appendix. In the next step, we calculated the degree of circular polarization according to

$$p_C = \frac{c \times \sin(\Delta_{CP}) \times \sin(2\varphi_{CP})}{b \times \cos(2\varphi_{CP}) - a}. \quad (10)$$

To measure the Müller matrix parameters of our circular polarizer, we placed it between the linear polarizer and analyzer and independently rotated both circular polarizer and analyzer around the beam axis. We applied the same measurement technique as for the linear polarizer, i.e., the photodiode signal was amplified with a low-noise current amplifier by a factor of 10^9 V/A and the resulting voltage was measured by a time-integrating voltmeter. We fixed the rotation angle φ_{CP} (counterclockwise with respect to the beam direction) and scanned φ_A (clockwise with respect to the beam direction) between 0° and 360° in 20° steps. For accurate polarization analysis, we separately measured the voltage offset for each φ_A with the EUV light source being off. A representative result for $\varphi_{CP} = 30°, 70°$, and 330° is displayed in Fig. 6(b). The periodic voltage modulations present for $\varphi_{CP} = 30°$ and $\varphi_{CP} = 330°$ disappear when $\varphi_{CP} = 70°$, i.e., the photodiode signal does not depend on the analyzer angle φ_A. For this rotation angle, we efficiently convert linearly to circularly polarized light at 60.5 eV as expected from simulations (Sec. II A). From measurements at six different angles φ_{CP}, we determined the parameters a, b, and c and derived a maximum value of $p_C = 0.81 \pm 0.15$ for $\varphi_{CP} = 70°$ and $\Delta_{CP} = -90.9°$.

V. XMCD MEASUREMENTS ON A Co/Pt-MULTILAYER FILM AT THE COBALT 3*p* ABSORPTION EDGE (60 eV)

For the XMCD studies, we placed the coil and magnetic yoke with a bore hole for transmission measurements directly behind the Bragg mirror linear and circular polarizers and mounted the sample on two piezo-driven linear stages for vertical and horizontal movement in the center between the pole shoes of the yoke. As a suitable test sample for our XMCD measurements we chose [Co (0.8 nm)/Pt (1.4 nm)]$_{16x}$ layers grown on Si_3N_4 (50 nm)/Pt(5 nm) by ion beam sputtering[25,26] and capped with Pt (0.6 nm). A Co/Pt multilayer film exhibits a large perpendicular uniaxial anisotropy[25,26] and therefore, can be magnetized out-of-plane, which, for normal incidence of light, ensures a strong XMCD signal at the Co 3*p* absorption edge. From the scientific perspective, a Co/Pt multilayer film is a highly interesting ferromagnetic layer system for several reasons. Most importantly, within a certain thickness range of Co and Pt layers, the magnetization oriented perpendicular or even canted with respect to the film plane tends to split into many alternatingly oriented ferromagnetic domains with the average domain size of about 100 nm at zero external magnetic field.[25,26] The latter property renders Co/Pt multilayer films an ideal model system for studies of laser heating effects on the ferromagnetic domain structure employing high harmonics[27] as well as for studies of femtosecond magnetization dynamics of nanometer scale domains with a free-electron laser.[28,29]

The magnetization curve of the Co/Pt multilayer sample measured with polar magneto-optical Kerr effect (P-MOKE) is shown in the inset of Fig. 7. In order to saturate the magnetization, we applied 320 mT magnetic field perpendicular to the sample surface. In our measurements, we first set the circular polarizer to $\varphi_{CP} = 70°$ ($p_C = +1$), alternately applied ±320 mT magnetic field, and then recorded the transmitted signal $I^{\pm}(\pm 320\,\text{mT})$ on the CCD camera for both magnetic fields. We note that the actual image on the CCD camera is the beam profile after the Co/Pt multilayer sample including all oxygen spectral lines reflected by the Bragg mirror linear polarizer (Fig. 5(b)). For further data analysis, the signal was binned along one spatial direction in the region of interest. The difference of the transmitted intensity averaged over 50 measurements for each magnetic field (10 s or 200 pulses per measurement), is shown in Fig. 7. For the background-corrected XMCD asymmetry A_{XMCD} calculated according to equation

$$A_{XMCD} = \frac{I^+(+320\,\text{mT}) - I^-(-320\,\text{mT})}{I^+(+320\,\text{mT}) + I^-(-320\,\text{mT})}, \quad (11)$$

we obtained $A_{XMCD} = +(2.7 \pm 0.1)\,\%$.

After that, we changed the rotation angle of the circular polarizer to $\varphi_{CP} = 110°$ ($p_C = -1$) and repeated the above described measurement procedure. As expected for the XMCD effect, the difference signal (Fig. 7) and thus the asymmetry keeps the same magnitude but changes its sign. We measured $A_{XMCD} = -(2.8 \pm 0.1)\%$. To validate our data, we calculated the expected XMCD asymmetry from the magneto-optical absorption $\Delta\beta$ of the refractive index

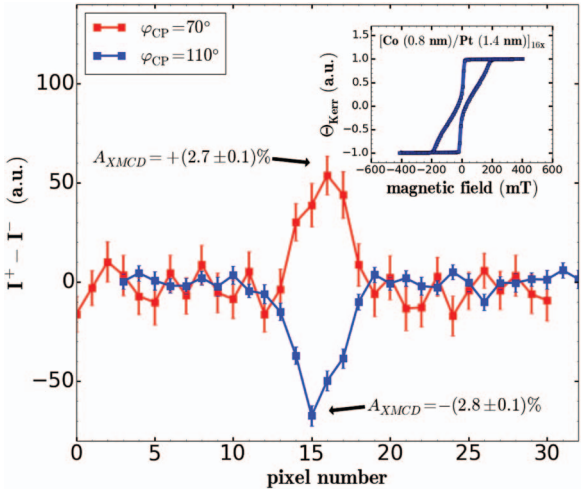

FIG. 7. XMCD difference signal $I^+(+320\,\text{mT}) - I^-(-320\,\text{mT})$ as recorded by the CCD camera for $\varphi_{CP} = 70°$ ($p_C = +1$) and $\varphi_{CP} = 110°$ ($p_C = -1$). We note that the graph displays a beam profile including all oxygen spectral lines reflected by the Bragg mirror linear polarizer (Fig. 5(b)). For the background-corrected XMCD asymmetry, we obtained $A_{XMCD} = +(2.7 \pm 0.1)\,\%$ and $A_{XMCD} = -(2.8 \pm 0.1)\,\%$ for different helicities. The inset shows the magnetization curve (Kerr rotation Θ_{Kerr}) of a [Co (0.8 nm)/ Pt (1.4 nm)]$_{16x}$ multilayer measured by polar magneto-optical Kerr effect (P-MOKE) with visible light (350 nm wavelength). Using our magnetic yoke with a maximum field of 320 mT the sample can be magnetized to saturation.

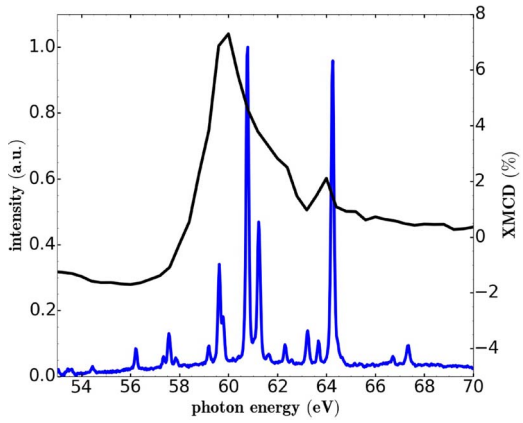

FIG. 8. XMCD spectrum for Co (total thickness $d = 12.8$ nm) calculated by Eq. (12) from experimentally determined imaginary part of magnetic refractive index[6] (black curve) and oxygen spectrum of the gas-discharge plasma-based EUV light source behind the Bragg mirror linear polarizer (blue curve).

$n = 1 - (\delta + \Delta\delta) + i \times (\beta + \Delta\beta)$ and a total Co thickness of $d = 12.8$ nm according to[4]

$$A_{XMCD} = 2\frac{E}{\hbar c} d \times \Delta\beta, \tag{12}$$

where E denotes the photon energy, $\hbar$ the reduced Planck constant, and c the speed of light. Contrary to other magneto-optical effects like the MOKE or the Faraday effect, the XMCD asymmetry depends on one single magneto-optical parameter $\Delta\beta$. To simulate A_{XMCD} in the vicinity of the Co $3p$ absorption edge, we inserted the photon energy-dependent parameter $\Delta\beta$ recently measured by Valencia *et al.*[6] in Eq. (12). The expected XMCD asymmetry is plotted together with the oxygen spectrum behind the Bragg mirror linear polarizer in Fig. 8. The expected asymmetry of a few percent agrees well with our data. We note that our XMCD signal represents an average over several spectral lines of the oxygen plasma (Fig. 5(b)).

To further confirm our results, we studied the magnetic field dependence of the intensity difference signal $I^+(\mu_0 H_{ref}) - I^-(\mu_0 H)$ defining a fixed reference magnetic field $\mu_0 H_{ref} = +320$ mT and six variable magnetic fields $\mu_0 H$ (−320 mT, −200 mT, −100 mT, 0 mT, 100 mT, and 200 mT). The intensity difference averaged over 10 measurements, each 10 s or 200 pulses, is displayed in Fig. 9.

As expected for $\mu_0 H_{ref} = +320$ mT from the magnetization curve (inset in Fig. 7), the difference signal is present for $\mu_0 H < 0$ and disappears for $\mu_0 H > 0$.

In summary, we generated circularly polarized light with both helicities from a laboratory-based plasma EUV light source and measured XMCD asymmetry values at the Co $3p$ absorption edge comparable to the reported synchrotron studies.[5,6] The changing sign of the XMCD asymmetry upon helicity reversal confirms the magnetic origin of the signal. Moreover, we changed the magnetic field and observed a magnetic signal, which follows the magnetization curve. Our results, to our knowledge, are the first laboratory-based XMCD measurements at the Co $3p$ absorption edge with a plasma-based EUV light source.

VI. CONCLUSION AND OUTLOOK

We simulated, designed, and characterized an instrument for generation of circularly polarized EUV light at the $3p$ absorption edges of Fe, Co, and Ni (50 eV–70 eV) employing a compact gas-discharge plasma-based EUV light source. For the first time in a laboratory-based experiment with a plasma-based EUV light source, we successfully measured the XMCD effect at the Co $3p$ absorption edge (60.5 eV) that previously was only possible at synchrotrons, at free-electron lasers and with laser-generated high harmonics due

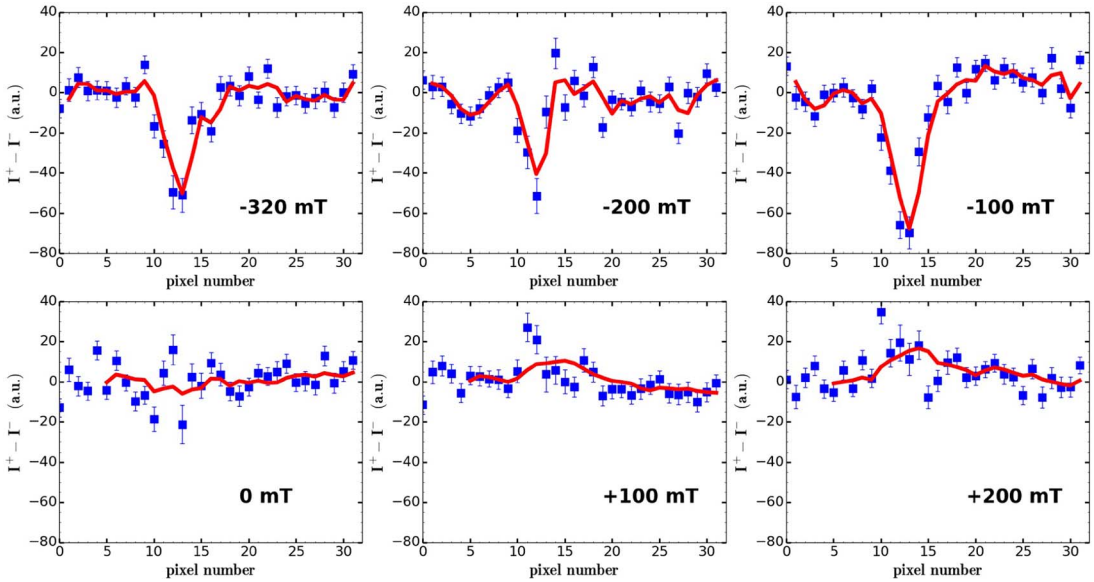

FIG. 9. Magnetic field dependence of the XMCD difference signal $I^+(\mu_0 H_{ref}) - I^-(\mu_0 H)$ (blue: data points, red: smoothed curve) for $\mu_0 H = -320$ mT, −200 mT, −100 mT, 0 mT, +100 mT, and +200 mT for a fixed reference magnetic field $\mu_0 H_{ref} = +320$ mT. Here, we fixed φ_{CP} to 110°. The XMCD difference signal is only present for $\mu_0 H < 0$, i.e., for different signs of $\mu_0 H_{ref}$ and $\mu_0 H$ as expected from the magnetization curve (inset in Fig. 7). For $\mu_0 H > 0$, i.e., for the same sign of $\mu_0 H_{ref}$ and $\mu_0 H$, no magnetic signal is expected according to the magnetization curve.

to the lack of circularly polarized EUV radiation in the small-scale laboratory. Our results open the perspective for transfer of some synchrotron capabilities to the home laboratory using full time available high power plasma-based light sources. These light sources offer the advantages of photon energies in the EUV and soft X-ray spectral range at high intensity with multi-kHz repetition rate. The spectral position and intensity of the emission lines can be tuned by gas species and electrical discharge energy, which immediately allows elemental and chemical contrast at elemental absorption edges. In addition, our work demonstrates that the initially unpolarized light is easily converted to linearly and circularly polarized light required for magneto-optical polarization spectroscopy and microscopy. In future studies, it is straightforward to combine our polarization optics and a Fresnel zone plate EUV microscope.[30] In our concept, the polarization optics will be placed between the collector and the ferromagnetic sample, which domain structure will be imaged by the Fresnel zone plate. The proposed microscope will significantly advance the current imaging techniques and allow element-selective imaging of ferromagnetic domains at the 3*p* absorption edges of Fe, Co, and Ni in the small-scale laboratory environment.

ACKNOWLEDGMENTS

L.J. acknowledges financial support by the Helmholtz Association for a Helmholtz Professorship as a part of the Pact for Research and Innovation. D.W., D.R., R.A., and L.J. also acknowledge financial support by JARA-FIT Seed Funds through the Excellence Initiative. Moreover, we thank Stefan Braun (Fraunhofer IWS Dresden) for Bragg mirror design and fabrication as well as Konstantin Tsigutkin for careful proofreading of the paper.

APPENDIX: CALCULATION OF p_C

The parameters a and b from Eq. (8) depend on the ellipsometric quantities ψ (see Eq. (4)) of all three Mo mirrors of the circular polarizer in the following way:

$$a = 1 + 2 \times \cos(2\psi_{40}) \times \cos(2\psi_{20}) + \cos(2\psi_{20})^2,$$

$$b = -2 \times \cos(2\psi_{20}) - \cos(2\psi_{40}) - \cos(2\psi_{40}) \times \cos(2\psi_{20})^2, \quad \text{(A1)}$$

where ψ_{20} and ψ_{40} denote the ellipsometric quantities for 20° and 40° grazing incidence, respectively. We solved this system of two nonlinear equations numerically for a fixed range of ψ_{20} and ψ_{40} and obtained ψ_{20} and ψ_{40} from measured parameters a and b (Sec. IV). Then, we calculated the parameter c according to equation

$$c = \sin(2\psi_{20})^2 \times \sin(2\psi_{40}) \quad \text{(A2)}$$

and, based on Eqs. (A1) and (A2) we derived the degree of circular polarization p_C using Eq. (10).

[1] D. Attwood, *Soft X-rays and Extreme Ultraviolet Radiation: Principles and Applications* (Cambridge University Press, 1999).
[2] F. Scholze, C. Laubis, C. Buchholz, A. Fischer, S. Plöger, F. Scholz, and G. Ulm, Proc. SPIE **6151**, 615137 (2006).
[3] S. Danylyuk, H.-S. Kim, P. Loosen, K. Bergmann, and L. Juschkin, J. Micro/Nanolith. MEMS MOEMS **12**(3), 033002 (2013).
[4] H.-Ch. Mertins, S. Valencia, A. Gaupp, W. Gudat, P. M. Oppeneer, and C. M. Schneider, Appl. Phys. A **80**, 1011 (2005).
[5] M. F. Tesch, M. C. Gilbert, H.-Ch. Mertins, D. E. Bürgler, U. Berges, and C. M. Schneider, Appl. Opt. **52**(18), 4294 (2013).
[6] S. Valencia, A. Gaupp, W. Gudat, H.-C. Mertins, P. M. Oppeneer, D. Abramsohn, and C. M. Schneider, New J. Phys. **8**, 254 (2006).
[7] L. Baumgarten, C. M. Schneider, H. Petersen, F. Schäfers, and J. Kirschner, Phys. Rev. Lett. **65**, 492 (1990).
[8] F. U. Hillebrecht, Ch. Roth, H. B. Rose, M. Finazzi, and L. Braicovich, Phys. Rev. B **51**, 9333 (1995).
[9] F. Schäfers, H.-Ch. Mertins, A. Gaupp, W. Gudat, M. Mertin, I. Packe, F. Schmolla, S. Di Fonzo, G. Soullié, W. Jark, R. Walker, X. Le Cann, R. Nyholm, and M. Eriksson, Appl. Opt. **38**(19), 4074 (1999).
[10] T. Imazono, K. Sano, Y. Suzuki, T. Kawachi, and M. Koike, Rev. Sci. Instrum. **80**(8), 085109 (2009).
[11] S. Kitamoto, H. Murakami, Y. Shishido, N. Gotoh, T. Shibata, K. Saito, T. Watanabe, J. Kanai, E. Takenaka, K. Nagasaki, M. Yoshida, D. Takei, and M. Morii, Rev. Sci. Instrum. **81**, 023105 (2010).
[12] H. C. Kapteyn, M. M. Murnane, and I. P. Christov, Phys. Today **58**(3), 39 (2005).
[13] W. B. Westerveld, K. Becker, P. W. Zetner, J. J. Corr, and J. W. McConkey, Appl. Opt. **24**, 2256 (1985).
[14] B. Vodungbo, A. Barszczak Sardinha, J. Gautier, G. Lambert, C. Valentin, M. Lozano, G. Iaquaniello, F. Delmotte, S. Sebban, J. Lüning, and P. Zeitoun, Opt. Express **19**(5), 4346 (2011).
[15] O. Kfir, P. Grychtol, E. Turgut, R. Knut, D. Zusin, D. Popmintchev, T. Popmintchev, H. Nembach, J. M. Shaw, A. Fleischer, H. Kapteyn, M. Murnane, and O. Cohen, e-print arXiv:1401.4101.
[16] H. Höchst, R. Patel, and F. Middleton, Nucl. Instrum. Methods Phys. Res. A **347**(1–3), 107 (1994).
[17] M. Suzuki, K. Hanmura, T. Kotani, N. Yamaguchi, M. Kobayashi, and A. Misu, Rev. Sci. Instrum. **66**, 1589 (1995).
[18] K. Bergmann, G. Schriever, O. Rosier, M. Müller, W. Neff, and R. Lebert, Appl. Opt. **38**, 5413 (1999).
[19] M. Benk and K. Bergmann, J. Micro/Nanolith. MEMS MOEMS **11**(2), 021106 (2012).
[20] K. Bergmann, S. V. Danylyuk, and L. Juschkin, J. Appl. Phys. **106**, 073309 (2009).
[21] H. Fujiwara, *Spectroscopic Ellipsometry* (Wiley, 2007).
[22] B. L. Henke, E. M. Gullikson, and J. C. Davis, At. Data Nucl. Data Tables **54**(2), 181 (1993); see http://henke.lbl.gov/optical_constants/, from this database, we extracted the refractive indices of Mo, Si, SiO_2, and B_4C between 50 eV and 70 eV photon energy.
[23] V. G. Horton, E. T. Arakawa, R. N. Hamm, and M. W. Williams, Appl. Opt. **8**(3), 667 (1969).
[24] K. Rabinovitch, L. R. Canfield, and R. P. Madden, Appl. Opt. **4**(8), 1005 (1965).
[25] H. Stillrich, C. Menk, R. Frömter, and H. P. Oepen, J. Appl. Phys. **105**, 07C308 (2009).
[26] D. Stickler, R. Frömter, H. Stillrich, C. Menk, H. P. Oepen, C. Gutt, S. Streit-Nierobisch, L.-M. Stadler, G. Grübel, C. Tieg, and F. Yakhou-Harris, Phys. Rev. B **84**, 104412 (2011).
[27] C. Weier, R. Adam, D. Rudolf, R. Frömter, P. Grychtol, G. Winkler, A. Kobs, H. P. Oepen, H. C. Kapteyn, M. M. Murnane, and C. M. Schneider, "Femtosecond-laser-induced modifications in Co/Pt multilayers studied with tabletop resonant magnetic scattering," Europhys. Lett. (submitted).
[28] B. Vodungbo, J. Gautier, G. Lambert, A. B. Sardinha, M. Lozano, S. Sebban, M. Ducousso, W. Boutu, K. Li, B. Tudu *et al.*, Nat. Commun. **3**, 999 (2012).
[29] S. Pfau, S. Schaffert, L. Müller, C. Gutt, A. Al-Shemmary, F. Büttner, R. Delaunay, S. Düsterer, S. Flewett, R. Frömter *et al.*, Nat. Commun. **3**, 1100 (2012).
[30] P. W. Wachulak, A. Bartnik, and H. Fiedorowicz, Opt. Lett. **35**(14), 2337 (2010).